ences because the reactions for R = *t*-Bu and *n*-Bu differ by approximately 3 orders of magnitude in k_{obsd}, yet the pK_a values for their corresponding parent amines are almost equivalent.[19] Therefore, it is concluded that for L = R-pyca the pyridine nitrogen atom initially scavenges the $W(CO)_5S$ photoproduct and that the slow chelation reaction occurs via the coordination of the aliphatic nitrogen atom. Contrastingly, when L = R-pyca', the kinetic data illustrate little dependence on the ligand substituent group R (see Table II). Thus, it is concluded that for L = R-pyca' the aliphatic nitrogen atom initially scavenges the $W(CO)_5S$ photoproduct and the ring closure process involves coordination by the pyridine nitrogen atom.

Figure 3 depicts the stereochemistries of two possible monodentate $W(CO)_5L$ intermediates. The diimine ligands are shown in a trans configuration as both theoretical and experimental studies on related systems have concluded that the free ligands exist in this conformation as solids and in solution.[20] Rotation about the C_2–C_2' bond is needed to produce the cis chelation arrangement, although this energy barrier may be rather small as it has been calculated to be between 20 and 28 kJ mol^{-1} for other diimines.[20g] Structure A illustrates the monodentate $W(CO)_5L$ intermediate that results when the aliphatic nitrogen atom of the ligand has scavenged the $W(CO)_5S$ photoproduct. It is noted that this arrangement involves substantial steric hindrance and electronic repulsion by the interaction of the pyridine ring with the carbonyl ligands. Structure B depicts the monodentate $W(CO)_5L$ intermediate that is formed when the initial scavenging takes place at the pyridine nitrogen atom, and it can be seen that this conformation involves much less steric hindrance. Hence, the observed kinetic data suggesting exclusive formation of structure B for the $W(CO)_5$(R-pyca) intermediates may be rationalized on the basis of steric constraint. On the other hand, for L = R-pyca' the kinetic results imply that structure A is predominantly formed, presumably because the methyl group precludes initial coordination at the pyridine nitrogen atom.

The ligand scavenging observations are also in accordance with this reasoning. This is because when L = R-pyca, the initial scavenging of $W(CO)_5S$ by L was seen to be efficient and take place rapidly, and when L = R-pyca', the scavenging was relatively slow and it suffered competition from solvent impurities. It is striking that the increased steric hindrance about the pyridine nitrogen atom in R-pyca' has such a significant effect on the ability of this ligand (even at 10^{-2} M) to scavenge $\sim 10^{-4}$ M of the $W(CO)_5S$ photoproduct, whereas extremely poor donor ligands such as N_2 or Ar can scavenge the unsaturated $W(CO)_5$ species at near diffusion-controlled rates.[14c,d] The results presented here clearly demonstrate that the steric properties of the entering ligand is a major factor in determining the scavenging mechanism of the $W(CO)_6$ primary photoproduct.

Acknowledgment. We are grateful to the donors of the Petroleum Research Fund, administered by the American Chemical Society, for supporting this research and thank Dorene Price for assistance with the kinetic measurements.

Registry No. *n*-Bu-pyca, 7032-24-8; *i*-Pr-pyca, 7032-23-7; Ph-pyca, 7032-25-9; *t*-Bu-pyca, 21478-42-2; *n*-Bu-pyca', 71769-88-5; *i*-Pr-pyca', 78004-29-2; Ph-pyca', 27768-36-1; *t*-Bu-pyca', 106155-16-2; $W(CO)_6$, 14040-11-0; $W(CO)_5$(*n*-Bu-pyca), 107339-94-6; $W(CO)_5$(*i*-Pr-pyca), 107339-93-5; $W(CO)_5$(Ph-pyca), 102190-24-9; $W(Co)_5$(*t*-Bu-pyca), 102190-23-8; $W(CO)_5$(*n*-Bu-pyca'), 117203-02-8; $W(CO)_5$(*i*-Pr-pyca'), 117203-03-9; $W(CO)_5$(Ph-pyca'), 117203-04-0; $W(CO)_5$(*t*-Bu-pyca'), 117203-05-1; $W(CO)_4$(*n*-Bu-pyca), 107339-96-8; $W(CO)_4$(*i*-Pr-pyca), 36107-20-7; $W(CO)_4$(Ph-pyca), 36107-21-8; $W(CO)_4$(*t*-Bu-pyca), 107339-95-7; $W(CO)_4$(*n*-Bu-pyca'), 117203-06-2; $W(CO)_4$(*i*-Pr-pyca'), 117203-07-3; $W(CO)_4$(*t*-Bu-pyca'), 117203-08-4; $W(CO)_4$(Ph-pyca'), 117203-09-5.

(19) Rappoport, Z., Ed. *CRC Handbook of Tables for Organic Compound Identification*, 3rd ed.; CRC: Boca Raton, FL, 1967; p 436.

(20) (a) Nakamoto, K. *J. Phys. Chem.* **1960**, *64*, 1420. (b) Cumper, C. W. N.; Ginman, R. F. A.; Vogel, A. *J. Chem. Soc.* **1962**, 1188. (c) Cureton, P. H.; LeFevre, C. G.; LeFevre, R. J. W. *J. Chem. Soc.* **1963**, 1736. (d) Castellano, S.; Gunther, H.; Ebersole, S. *J. Phys. Chem.* **1965**, *69*, 4166. (e) Spotswood, T. McL.; Tanzer, C. I. *Aust. J. Chem.* **1967**, *20*, 1227. (f) Kliegman, J. M.; Barnes, R. K. *Tetrahedron Lett.* **1969**, 1953. (g) Benedix, R.; Birner, P.; Birnstock, F.; Hennig, H.; Hofmann, H.-J. *J. Mol. Struct.* **1979**, *51*, 99.

Laser–Ion Beam Photodissociation Studies of Ionic Cluster Fragments of Iron Carbonyls: $Fe_x(CO)_y^+$ (x = 1–3; y = 0–6)

R. E. Tecklenberg, Jr., D. L. Bricker, and D. H. Russell*

Department of Chemistry, Texas A&M University, College Station, Texas 77840

Received March 18, 1988

Ionic cluster fragments of the type $Fe_x(CO)_y^+$ (x = 1–3; y = 0–6) are mass resolved by high-resolution mass spectrometry (R = 7500) and then photodissociated. The photofragment ions are mass analyzed by an electrostatic analyzer. The ions studied include $Fe(CO)_y^+$ (y = 1–5), $Fe_2(CO)_y^+$ (y = 0–6), and $Fe_3(CO)_y^+$ (y = 0–4) derived from $Fe_3(CO)_{12}$ neutral. Relative photofragment ion yields for each photodissociating ion and upper and lower limits to the average bond dissociation energies for both Fe^+–CO and Fe^+–Fe bonds are reported. Average metal–ligand binding energies in the range 19.5–58.6 kcal/mol are measured for iron–carbonyl bonds. The photodissociation threshold for $Fe_3^+ \rightarrow Fe_2^+ + Fe$ is found to be <27.8 kcal/mol. The Fe_2^+ ion does not photodissociate over the wavelength range (458–514.5 nm), placing the lower limit for the bond dissociation energy at <62.4 kcal/mol.

Introduction

The chemical and physical properties of ionic transition-metal species, e.g., monatomic bare and ligated metals, as well as dimer, trimer, and small metal clusters, have been the subject of intense research over the past decade.[1-6] There have been numerous recent studies that demonstrate the change in chemical reactivities as a function of

(1) Armentrout, P. B.; Beauchamp, J. L. *J. Am. Chem. Soc.* **1981**, *103*, 6628.

0276-7333/88/2307-2506$01.50/0

cluster size and the dependence of the chemical reactions on the electron environment. For instance, niobium clusters, Nb_n^+, show a remarkable size dependence for reaction with H_2.[7] Ridge has compared the reactivity of Co^+, Co_2^+, and $Co_2(CO)^+$ and attributed the different reactivities for $Co_2(CO)^+$ and Co_2^+ to electronic effects of the CO ligand.[8] Recent studies also clearly indicate the existence of long-lived electronic states of metal ions and the importance of these species on chemical reactivities. For example, Ridge and Freas have shown that the excited state of Cr^+ gives rise to $CrCH_2^+$ (CH_4 reacting neutral),[9] and these authors suggest that it is the excited state of Cr^+ that reacts with butane.[10] Armentrout has studied the reactivity of ground-state (^6D) Fe^+ and excited-state (^4F) Fe^+ with H_2 and presented convincing evidence that ground-state Fe^+ is much less reactive (a factor of 80) to form FeH^+.[11] These studies demonstrate the need for additional information on the physical properties of transition-metal species, and how such properties influence the chemical reactivities of these species.

In a series of three papers we described ion–molecule reaction chemistry methods for the preparation of novel, highly coordinatively unsaturated ionic cluster fragments of the type $M_x(CO)_y^+$ (M = Cr, Fe, Co, Ni: x = 2–8; y = 0–3x) and heteronuclear analogues of similar composition.[2,12,13] Relating the rate of formation of ion–molecule reaction product ions to their electron deficiencies has proven useful in obtaining information on chemical structure and bonding properties of transition-metal cluster fragment ions.[14,15] Our interest in the ionic cluster fragments stems from the ability to probe the changes in the chemical and physical properties of such systems as a function of cluster size and metal-to-ligand ratio.[16] In a later publication we reported on the laser ion beam photodissociation of $M_x(CO)_y^+$ ion cluster fragments where M = Mn, Fe, and Co.[17] This work concentrated on relative photodissociation cross sections, branching ratios for various photofragment ions, and estimates of the upper limits of metal–metal and metal–ligand bond energies. For the $Fe_3(CO)_y^+$ ions (y = 5–12) metal–metal bond energies could not be obtained because the dominant photofragment ions formed correspond to expulsion of carbonyl ligands. Average metal–metal bond dissociation energies for the $Mn_2(CO)_y^+$ (y = 0–10) and $Co_4(CO)_y^+$ (y = 0–12) are <44 kcal/mol and 16 kcal/mol, respectively. Large variations in the metal–ligand bond energies were obtained. For example, Mn^+–CO bond energies range from <10 kcal/mol to ca. 20 kcal/mol for ions having large metal-to-ligand ratios (e.g. $Mn_2(CO)^+$). In the cobalt system metal–ligand bond energies averaged 23 kcal/mol and the deviation from this value was small, ca. 0.5 kcal/mol. In the case of $Fe_x(CO)_y^+$, the metal–ligand bond energies were ca. 20–23 kcal/mol except for $Fe_3(CO)_5^+$ which has a Fe^+–CO bond energy of 45 kcal/mol. The photodissociation studies of $Fe_x(CO)_y^+$ (x = 1–3; y = 0–4) is complicated by the overlap in masses for ^{56}Fe and $(CO)_2$. For example, the signal at nominal mass 196 is composed of a triplet of ions which corresponds to $Fe_3(CO)^+$, $Fe_2(CO)_3^+$, and $Fe(CO)_5^+$. This problem prohibited us from studying the photochemistry of $Fe_x(CO)_y^+$ (i.e. x = 1–3; y = 0–6) species with large metal-to-ligand ratios in our earlier publication.[17]

In this paper, the photochemistry of the $Fe(CO)_y^+$ (y = 1–4), $Fe_2(CO)_y^+$ (y = 0–6), and $Fe_3(CO)_y^+$ (y = 0–4) ions mass-selected by high-resolution mass spectrometry is reported. Branching ratios for photochemical reaction channels are reported as well as upper limits for metal–metal and metal–ligand bond energies. In general, the metal–ligand bond energies for the $Fe_x(CO)_y^+$ species follow the same general trend as observed for $Mn_x(CO)_y^+$ and $Co_x(CO)_y^+$ systems. That is, low metal–ligand bond energies of ca. 20 kcal/mol for small x/y ratios and metal–ligand bond energies which increase to as much as 58 kcal/mol for $x/y \geq 1$. Upper limits to the metal–metal bond energies for Fe_3^+ ion and lower limits to the metal–metal bond energy for the Fe_2^+ ion are determined (<28 and >62 kcal/mol, respectively). These metal–metal bond energies determined are in agreement with those reported by Smalley.[18]

Experimental Section

All laser–ion beam photodissociation experiments were performed on a triple analyzer Kratos MS-50 TA mass spectrometer (see Figure 1). The instrument and the experimental procedures were described in detail in an earlier paper.[17] For the purposes of this paper the important details are associated with MS-I. That is, the first electrostatic analyzer (ESA) and the magnet comprise a high-resolution (maximum resolving power ca. 150 000) instrument. The practical utility of an instrument with ultra-high-resolution capabilities is that high sensitivities can be maintained at moderate resolutions, e.g., 8 000–20 000 resolving power. The second electrostatic analyzer is then used for kinetic energy analysis of the photofragment ions. The kinetic energy of the photofragment ions can be related to the m/z ratio by the relationship; $m_2^+ = m_1^+(E_2/E_1)$, where m_2^+ is the m/z value of the photofragment ion, m_1^+ is the m/z value for the incident ion, E_2 is the electrostatic analyzer voltage necessary to pass m_2^+, and E_1 is the electrostatic analyzer voltage necessary to pass m_1^+.

Ions are produced by electron-impact (EI) ionization using an ionizing energy of 70 eV. The visible lines (514.5–458 nm) of an argon ion laser (Coherent Model CR-18) are used for all photodissociation experiments described herein. Mirrors M1, M2, and M5 (see Figure 1) are used to direct the laser beam through a sapphire window in the third field-free region where the laser beam and ion beam are crossed in an orthogonal fashion. A 300-mm focal length sapphire lens is used to focus the laser beam to a small point (0.1–0.3 mm in diameter) just at the laser–ion beam intersection. Photodissociation is performed within 1 cm of the focal point of MS-I, where the dimensions of the ion beam are small (<0.25 mm). Therefore, focusing the laser beam to dimensions that are equal to or slightly less than the dimensions of the ion beam give marked enhancements in the photofragment ion yields. Photofragment ions formed between the magnetic analyzer and second electrostatic analyzer are energy analyzed by using standard MIKE scans.[19–21] The laser beam is mechanically

(2) Fredeen, D. A.; Russell, D. H. *J. Am. Chem. Soc.* **1985**, *107*, 3762.
(3) Lane, K. R.; Sallans, L.; Squires, R. R. *J. Am. Chem. Soc.* **1985**, *107*, 5369.
(4) Jacobson, D. B.; Freiser, B. S. *J. Am. Chem. Soc.* **1986**, *108*, 27.
(5) Stevens, A. E.; Feigerle, C. S.; Lineberger, W. C. *J. Am. Chem. Soc.* **1982**, *104*, 5026.
(6) Jarrold, M. F.; Misev, L.; Bowers, M. T. *J. Phys. Chem.* **1984**, *88*, 3928.
(7) Elkind, J. L.; Weiss, F. D.; Alford, J. M.; Laaksonen, R. T.; Smalley, R. E. *J. Chem. Phys.*, in press.
(8) Freas, R. B.; Ridge, D. P. *J. Am. Chem. Soc.* **1984**, *106*, 825.
(9) Reents, W. D., Jr.; Strobel, F.; Freas, R. B., III; Wronka, J.; Ridge, D. P. *J. Phys. Chem.* **1985**, *89*, 5666.
(10) Armentrout, P. B.; Halle, L. F.; Beauchamp, J. L. *J. Am. Chem. Soc.* **1981**, *103*, 6501.
(11) Elkind, J. L.; Armentrout, P. B. *J. Am. Chem. Soc.* **1986**, *108*, 2765.
(12) Fredeen, D. A.; Russell, D. H. *J. Am. Chem. Soc.* **1986**, *108*, 1860.
(13) Fredeen, D. A.; Russell, D. H. *J. Am. Chem. Soc.* **1987**, *109*, 3903.
(14) Ridge, D. P.; Meckstroth, W. K. In *Modern Inorganic Chemistry, Gas Phase Organometallic Chemistry*; Russell, D. H., Ed.; Plenum: New York, in preparation.
(15) Wronka, J.; Ridge, D. P. *J. Am. Chem. Soc.* **1984**, *106*, 67.
(16) Mutterties, E. L.; Rhodin, T. N.; Band, E.; Brucker, C. F.; Pretzer, W. R. *Chem. Rev.* **1979**, *79*, 91.
(17) Tecklenburg, R. E., Jr.; Russell, D. H. *J. Am. Chem. Soc.* **1987**, *109*, 7654.
(18) Brucat, P. J.; Zheng, L. S.; Pettiette, C. L.; Yang, S.; Smalley, R. E. *J. Chem. Phys.* **1986**, *84*, 3078.

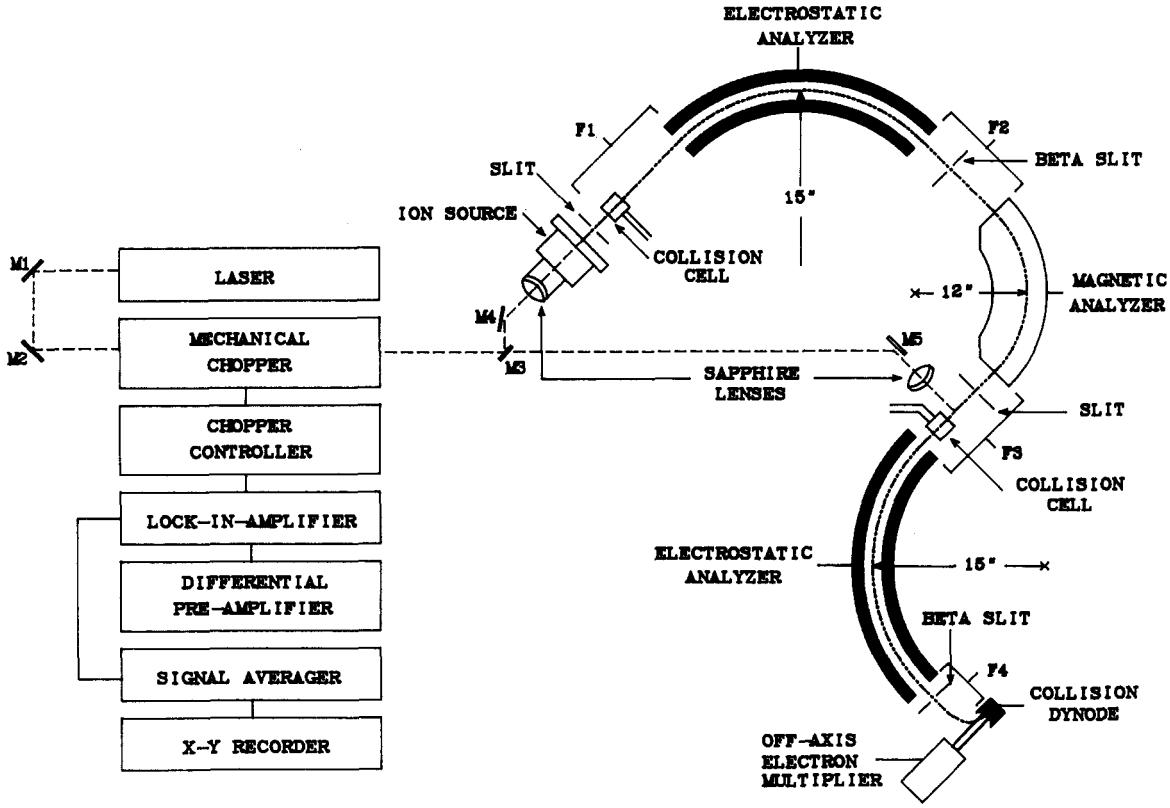

Figure 1. Schematic diagram of the laser–ion beam photodissociation apparatus. The laser beam (dashed line) is overlapped perpendicularly with the ion beam in the third field-free region of the mass spectrometer by using mirrors M1, M2, and M5.

chopped at a frequency of 400 Hz, and the photoinduced signal is separated from metastable and collision-induced products by using a lock-in amplifier (Princeton Applied Research Model 124A) which measures the laser "on"/laser "off" difference signal. The difference signal is accumulated and signal-averaged by using a Model 1170 Nicolet signal averager until reasonable signal-to-noise ratios are obtained.

Although the mass resolution of MS-I is high (up to 150 000),[22] the mass resolution of MS-II is limited. The mass resolution is limited because the photofragment ions are energy analyzed and signal broadening can occur as a result of partitioning of internal energy as kinetic energy upon dissociation. Thus, it is not possible to distinguish loss of iron (m/z = 55.9349) from loss of two carbonyl ligands (m/z = 55.9898). To differentiate these two losses, photodissociation was performed on the ^{54}Fe isotope of a particular ion instead of the ^{56}Fe isotope, e.g. $^{54}Fe^{56}Fe_2(CO)_2^+$ (m/z = 222), instead of $^{56}Fe_3(CO)_2^+$ (m/z = 224). Assuming the ion at m/z = 222 loses iron and photodissociates in a statistical manner, then 33% of the ions will lose 54 mass units (^{54}Fe), while 67% of the ions will photodissociate by loss of 56 mass units (^{56}Fe). The results of these studies indicate that in cases where the identity of the daughter ion was uncertain (e.g. $Fe_x(CO)_y^+$ ions ($x \geq 2$; $y \geq 2$)), loss of two carbonyl ligands is the only photodissociation pathway observed (see Results and Discussion).

$Fe_3(CO)_{12}$ was purchased from Strem Chemical, Inc. (Newburyport, MA 01950). The sample was introduced into the mass spectrometer by a direct insertion solids probe. The direct insertion probe was heated to ~85 °C. This temperature is rather critical, since higher temperatures cause the sample to decarbonylate, and at lower temperatures the rate of sample sublimation is low. Because no measurable impurities were observed in the mass spectra of $Fe_3(CO)_{12}$, the sample was used without any purification.

Results and Discussion

This work investigates the single-photon photodissociation of $Fe_x(CO)_y^+$ ions (x = 1–3; y = 0–6) formed by electron-impact ionization of $Fe_3(CO)_{12}$ and subsequent mass selection by high resolution. The 70-eV low-resolution electron-impact ionization mass spectra of $Fe_3(CO)_{12}$ has previously been reported.[23] The high-resolution mass spectrum reveals the presence of the Fe_3^+ (m/z = 168) indicating that rupture of all metal carbonyl bonds is possible. Fe–Fe bonds of $Fe_3(CO)_{12}$ are also broken upon electron-impact ionization. That is, at m/z values ≤280, di- and monoiron carbonyl species are also observed in the mass spectrum. Mass doublets (m/z = 280, 252, 224, 140, 112) and triplets (m/z = 196, 168) are observed in the high-resolution mass spectrum of $Fe_3(CO)_{12}$: e.g., m/z = 196 corresponds to $Fe(CO)_5^+$, $Fe_2(CO)_3^+$, and $Fe_3(CO)^+$ ions. Figure 2 contains a portion of the high-resolution mass spectrum near mass 196 (MS-I mass resolution = 7500, 10% valley definition). These mass doublets and triplets require a minimum resolution of 4000–5000 for base-line separation of the individual ions. High resolution using ion-beam mass spectrometers is accomplished by narrowing mechanical slits, thereby attenuating the total ion current and instrument sensitivity. In the experiments described below the instrument resolution is set slightly above the minimum mass resolution required to completely separate the precursor ions.

Table I contains relative photodissociation cross sections for the cross-beam photodissociation of $Fe_x(CO)_y^+$ ions (x = 1–3; y = 0–5) as a function of laser wavelength. The

(19) Cooks, R. G.; Beynon, J. H.; Caprioli, R. M.; Lester, G. R. *Metastable Ions*; Elsevier: Amsterdam, London, New York, 1973.
(20) Gross, M. L.; Russell, D. H. *Tandem Mass Spectrometry*; McLafferty, F. W., Ed.; Wiley: New York, 1983; p 255.
(21) Russell, D. H.; Smith, D. H.; Warmack, R. J.; Bertram, L. K. *Int. J. Mass Spectrom. Ion Phys.* **1980**, *35*, 381.
(22) Gross, M. L.; Chess, E. K.; Lyon, P. A.; Crow, F. W.; Evans, S.; Tudge, H. *Int. J. Mass Spectrom. Ion Phys.* **1982**, *42*, 243.
(23) Lewis, J.; Manning, A. R.; Miller, J. R.; Wilson, J. M. *J. Chem. Soc. A* **1966**, 1663.

Table I. Photodissociation Cross Sections Measured from the Cross-Beam Photodissociation of $Fe_x(CO)_y^+$ Ions over the Wavelength Range 458–514 nm

precursor ion		photofragment Ion(s)	wavelength (nm) 458	476	488	496	502	514
$Fe_3(CO)_4^+$	→	$Fe_3(CO)_3^+$	0.00074	0.00057	0.00031	0.00011		
$Fe_3(CO)_3^+$	→	$Fe_3(CO)^+$	0.17	0.27	0.086	0.090	0.049	0.039
$Fe_3(CO)_2^+$	→	Fe_3^+	0.097	0.036	0.020	0.032	0.030	0.017
$Fe_3(CO)^+$	→	Fe_3^+	0.0069	0.0053	0.0050	0.0043	0.0036	0.0010
Fe_3^+	→	Fe_2^+	0.012	0.010	0.0051	0.0060	0.0078	0.0062
$Fe_2(CO)_5^+$	→	$Fe_2(CO)_3^+$	1.00	0.54	0.30	0.16	0.078	0.043
$Fe_2(CO)_4^+$	→	$Fe_2(CO)_2^+$	0.28	0.16	0.12	0.16	0.094	0.070
	→	$Fe_2(CO)^+$	0.167	0.125	0.026			
$Fe_2(CO)_3^+$	→	$Fe_2(CO)^+$	0.31	0.15	0.12	0.13	0.090	0.064
$Fe_2(CO)_2^+$	→	Fe_2^+	0.14	0.10	0.056			
$Fe_2(CO)^+$	→	Fe_2^+	0.023	0.0078	0.00080			
Fe_2^+	→	Fe^+						
$Fe(CO)_4^+$	→	$Fe(CO)_2^+$	0.023	0.023	0.0098	0.0063	0.0043	0.0019

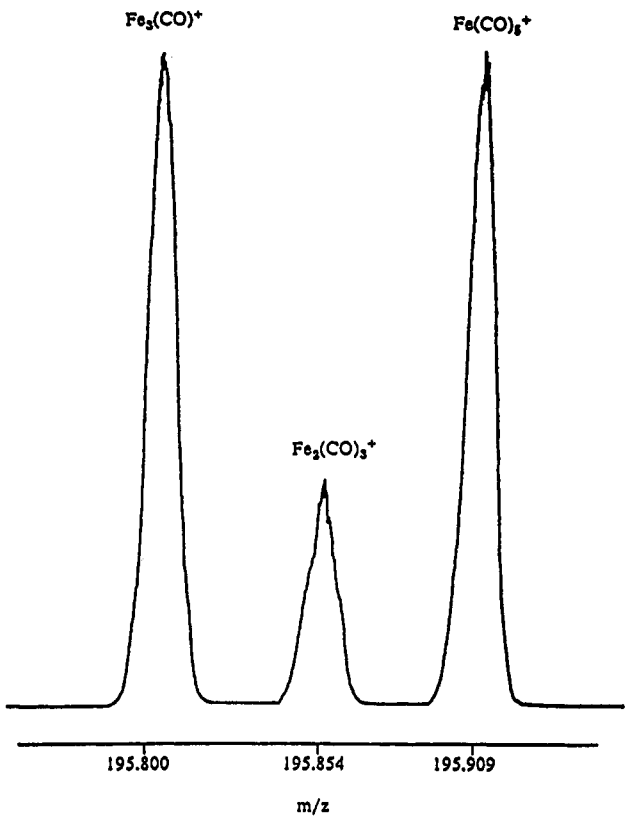

Figure 2. High mass resolution separation of the triplet of ions near m/z = 196 prior to photoactivation in the third field-free region of the mass spectrometer (R = 7500, 10% valley definition).

relative photodissociation cross sections are normalized for laser power, ion collector signals, and photofragment peak heights as described previously.[17] Photodissociation cross section measurements for each iron cluster ion are normalized to the photodissociation reaction having the largest cross section (i.e. $Fe_2(CO)_5^+ \rightarrow Fe_2(CO)_3^+$). For example, in Table I loss of two carbonyl ligands from $Fe_2(CO)_5^+$ is found to have the largest relative photofragment ion yield at λ = 458 nm, and this reaction is assigned a photodissociation cross section of 1.00. Therefore, all other photodissociating $Fe_x(CO)_y^+$ ions are normalized to this transition. Estimates of maximum uncertainty in the measured cross section values varied from ±15–20% for those iron carbonyl ions with small photodissociation cross sections to better than ±5% for ions with larger photodissociation cross sections.

In order to observe the photodissociation process $A^+ \rightarrow B^+ + C$, the ion must have a nonzero absorption cross section at the incident wavelength and the energy of the absorbed photon must be greater than the bond dissociation energy threshold(s).[24-26] If an excited electronic state of A^+ lies close to the dissociation threshold, the measured bond dissociation energy is said to be thermodynamically controlled and will reflect the true bond dissociation energy. In most cases the fortuitous overlap between the energies of the excited state and dissociation thresholds does not exist. However, Freiser and co-workers have suggested that for metal containing ions, a high density of low-lying electronic states may often times result in an overlap between excited states and dissociation thresholds.[25-27] Therefore, it should be emphasized that laser–ion beam photodissociation only provides estimates of the upper limits for bond dissociation energies.

Table II. Average Bond Dissociation Energies Measured from the Crossed Laser-Ion Beam Photodissociation Thresholds for $Fe_x(CO)_y^+$ Ions

transition	threshold nm	threshold kcal/mol	threshold energy no. of bonds broken (kcal/mol)
$Fe_3(CO)_4^+ \rightarrow Fe_3(CO)_3^+$	502	56.9	56.9
$Fe_3^+ \rightarrow Fe_2^+$	>514.5	<55.6	<27.8[a]
$Fe_3^+ \rightarrow Fe_2^+$	>514.5	<55.6	<55.6[b]
$Fe_2^+ \rightarrow Fe^+$	<458	>62.4	>62.4
$Fe_2(CO)_4^+ \rightarrow Fe_2(CO)^+$	488	58.6	19.5
$Fe_2(CO)_2^+ \rightarrow Fe_2^+$	488	58.6	29.3
$Fe_2(CO)^+ \rightarrow Fe_2^+$	488	58.6	58.6

[a] Triangular arrangement of three ion atoms assumed in the bond energy calculation. [b] Linear arrangement of three ion atoms assumed in the bond energy calculation.

The average bond dissociation energies reported in this paper are obtained by dividing the photodissociation threshold energy (disappearance of a photodissociation signal) by the number of ruptured metal–metal or metal–ligand bonds. Table II lists the average bond dissociation energies derived from the photodissociation thresholds for many of the $Fe_x(CO)_y^+$ ions, as well as the upper and lower limits to the bond dissociation energies for the Fe_3^+ and Fe_2^+ ions.

Figure 3 contains the photofragment ion spectrum for $Fe(CO)_4^+ \rightarrow Fe(CO)_2^+$ over the visible wavelength range 458–514.5 nm. The $Fe(CO)_4^+$ ion shows an apparent photodissociation maximum between 458 and 476 nm. The relative photodissociation cross sections for this transition are typical for the $Fe_x(CO)_y^+$ (x = 1–3) ions: i.e., large

(24) Dunbar, R. C. *Gas Phase Ion Chemistry*; Bowers, M. T., Ed.; Academic: New York, 1979; Vol. 2, p 181.
(25) Hettich, R. L.; Freiser, B. S. *J. Am. Chem. Soc.* **1985**, *107*, 6222.
(26) Hettich, R. L.; Jackson, T. C.; Stanko, E. M.; Freiser, B. S. *J. Am. Chem. Soc.* **1986**, *108*, 5086.
(27) Cassady, C. J.; Freiser, B. S. *J. Am. Chem. Soc.* **1984**, *106*, 6176.

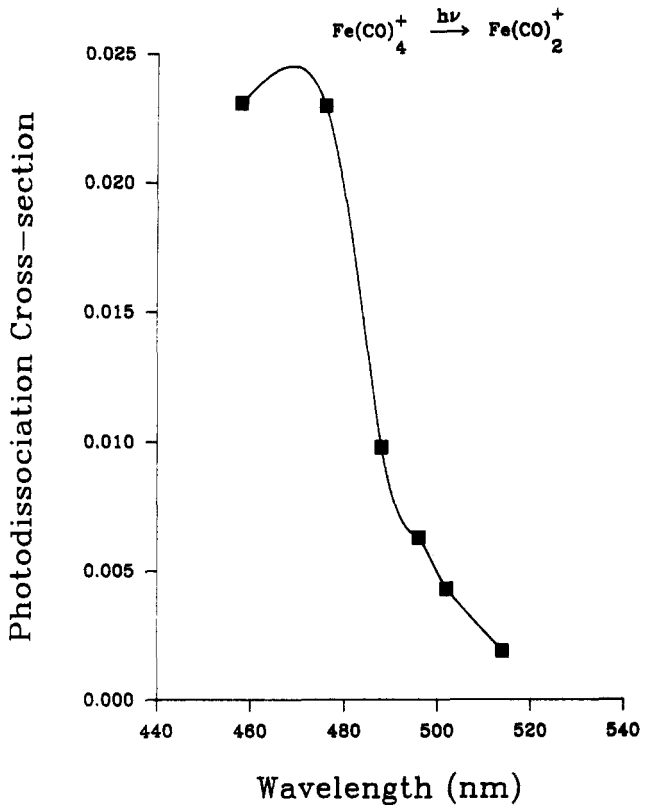

Figure 3. Photodissociation cross section as a function of laser wavelength for $Fe(CO)_4^+ \rightarrow Fe(CO)_2^+$.

photodissociation cross sections at high energies (458 nm) with smaller photodissociation cross sections at low energies (514.5 nm).[17]

It should be noted that the $Fe(CO)_4^+$ ion is the only monoiron carbonyl ion that photodissociates in the 458–514.5 nm range. There are three reasons why the $Fe(CO)_y^+$ ions (y = 1–3, 5) do not photodissociate in cross-beam experiment: (i) metal–ligand bond dissociation energies of $Fe(CO)_y^+$ (y = 1–3, 5) are quite high, i.e., >2.7 eV (63 kcal/mol); (ii) the $Fe(CO)_y^+$ ions (y = 1, 3–5) have low absorption cross sections in the blue-green wavelength region; (iii) the photoexcited $Fe(CO)_y^+$ ions (y = 1–3, 5) may dissociate slowly.

High metal–ligand bond energies for $Fe(CO)_y^+$ (y = 1–3, 5) are contradictory to that observed for the neutral species. For example, the accepted value for the binding energy for $Fe(CO)_4$–$CO \rightarrow Fe(CO)_4$ is ca. 2.4 eV, and the energy required for $Fe(CO)_5 \rightarrow Fe + 5(CO)$ is ca. 6.6 eV.[28] Thus, the average metal–ligand binding energy for the $Fe(CO)_4$ species is approximately 1 eV (23 kcal/mol).

Although the $Fe(CO)_y^+$ (y = 1–3, 5) ions do not photodissociate between 514.5 and 458 nm, relatively strong photodissociation transitions are observed in the all-line UV mode of the argon ion laser (333–385 nm with a weighted average of 355 nm). For example, $Fe(CO)_5^+$ photodissociates to $Fe(CO)_2^+$ upon absorption of a UV photon. Thus, an upper limit for the average metal–ligand bond dissociation energy of ca. 1.1 eV is indicated. The $Fe(CO)_3^+$ ion photodissociates (UV lines) to $Fe(CO)_2^+$ and $Fe(CO)^+$ with branching ratios for the photofragment ions of ~1/1; metal–ligand bond dissociation energies of <3.4 and 1.7 eV, respectively. $Fe(CO)_2^+$ gives exclusively Fe^+ upon UV photodissociation yielding an upper limit for the bond energy of 1.7 eV/carbonyl ligand. The $Fe(CO)^+$ ion photodissociates to Fe^+ suggesting a metal–ligand bond dissociation energy of <3.4 eV. Although the photodissociation of $Fe(CO)_4^+$ to yield $Fe(CO)_2^+$ is strong in the visible region, no additional photofragments are observed upon UV photodissociation. The clear trend that emerges from this data is that the metal–ligand bond dissociation energies for $Fe(CO)_y^+$ (y = 1–3, 5) do not exceed 1.7 eV and could be as low as 1.1 eV; $Fe(CO)^+$ is the only possible exception. Our results for the $Fe(CO)_y^+$ (y = 1–3, 5) are consistent with the photoionization mass spectrometry data reported by Distefano.[29] Therefore, absorption of a visible photon should produce a photoexcited ion with sufficient internal energy to fragment.

Information on the absorption properties of the $Fe(CO)_y^+$ (y = 1–5) ions can be extracted from coaxial laser–ion beam photodissociation experiments. Figure 4 shows the coaxial photofragment ion spectra for Fe^+, $Fe(CO)^+$, and $Fe(CO)_2^+$ ions obtained at visible wavelengths. That is, these spectra show all the parent ions that upon photoexcitation yield Fe^+, $Fe(CO)^+$, and $Fe(CO)_2^+$. There are several details to note in the spectra. (i) At 514.5 nm the yield for Fe^+ from $Fe(CO)^+$ is about three times that for $Fe(CO)_2^+$, but as the photon energy is increased, the $Fe(CO)_2^+ \rightarrow Fe^+$ reaction becomes dominant. A similar trend is noted for $Fe(CO)_3^+ \rightarrow Fe(CO)^+$ compared to $Fe(CO)_2^+ \rightarrow Fe(CO)^+$. (ii) Figure 5 contains data for the photodissociation of $Fe(CO)^+ \rightarrow Fe^+$ (514.5 nm) as a function of laser power. Note the square root dependence of the photofragment ion yield on the laser power. Our interpretation of this result is that photodissociation of $Fe(CO)^+$ to Fe^+ in the visible region corresponds to a two-photon process. However, this interpretation of the data should be regarded as preliminary. In the coaxial photodissociation studies, the laser beam and ion beam overlap over the entire length between the exit to the ion source and entrance to the first electrostatic analyzer (10–15 cm). Hence, the long laser–ion beam interaction distance may lead to sequential mutliphoton process. The laser powers used in these studies are not sufficient for photodissociation by a ladder mechanism; thus any multiphoton processes observed must occur via long-lived excited species, i.e., a sequential photon absorption mechanism.[30] Hence, the coaxial photodissociation experiments prove the $Fe(CO)_y^+$ (y = 1, 3–5) ions do indeed absorb in the blue-green wavelengths.

Proposing that $Fe(CO)_y^+$ (y = 1–3, 5) ions photodissociate via a sequential two-photon process has interesting implications. The question arises as to why the photoexcited $Fe(CO)_y^+$ ions, formed by absorption of the first visible photon, do not dissociate. For instance, the UV photodissociation results yield estimated metal–ligand bond dissociation energies of between 1.1 and 1.7 eV, consistent with Distefano photoionization mass spectrometry data.[29] The most logical explanation for the lack of photodissociation for the $Fe(CO)_y^+$ ions in the cross-beam experiment is that the spin state of the precursor ion does not correlate with the spin state of the photofragment ion; thus the photoexcited ion must relax via slow spin-forbidden dissociation channel. On the other hand, if the photoexcited ion is long-lived (ca. 1–5 μs in our experiment), absorption of a second photon could produce a highly excited ion which dissociates. It is also reasonable to suspect that the photoexcited $Fe(CO)_y^+$ ion (formed by absorption of one photon) decays by radiative processes which preempt dissociation. The details of photodissociation of $Fe(CO)_y^+$ ions is being probed further with this

(28) Lineberger, W. C. *J. Am. Chem. Soc.* **1979**, *101*, 5569.

(29) Distefano, G. *J. Res. Natl. Bur. Stand., Sect. A* **1970**, *74A*, 233.
(30) Freiser, B. S.; Beauchamp, J. L. *Chem. Phys. Lett.* **1975**, *35*, 35.

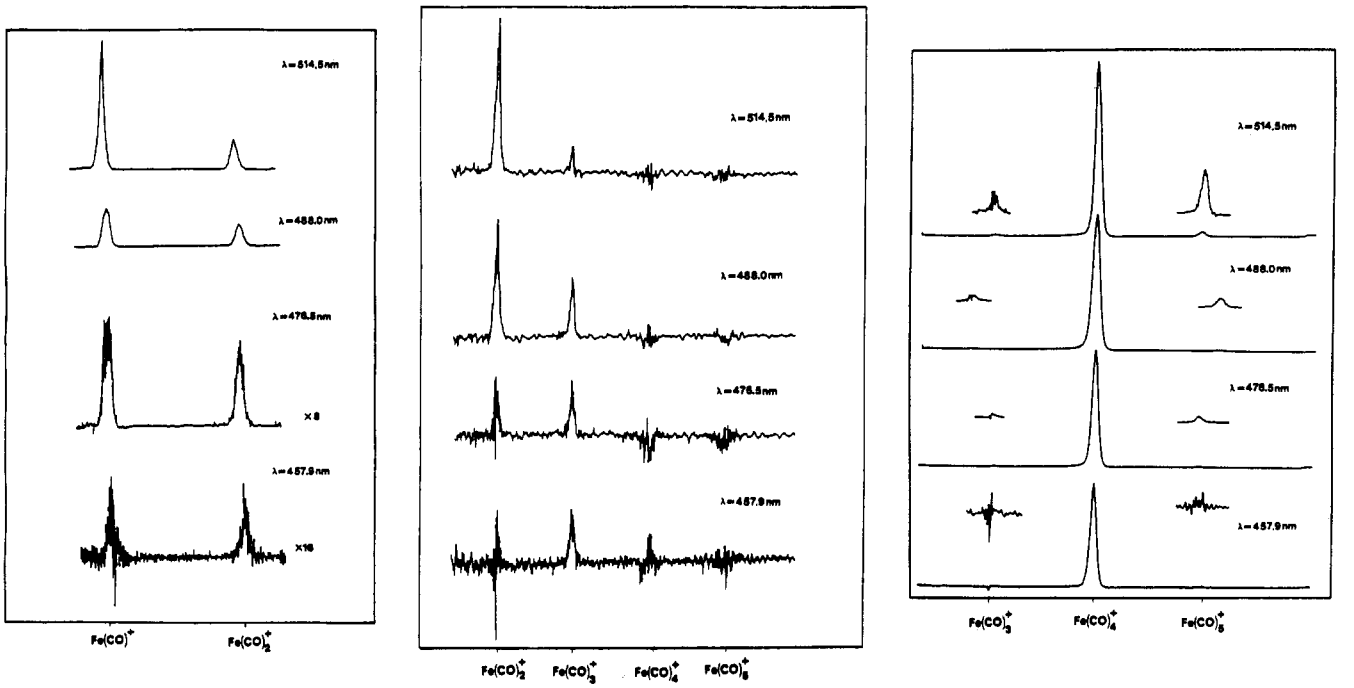

Figure 4. Coaxial photofragment ion spectra for Fe^+, $Fe(CO)^+$, and $Fe(CO)_2^+$ ions.

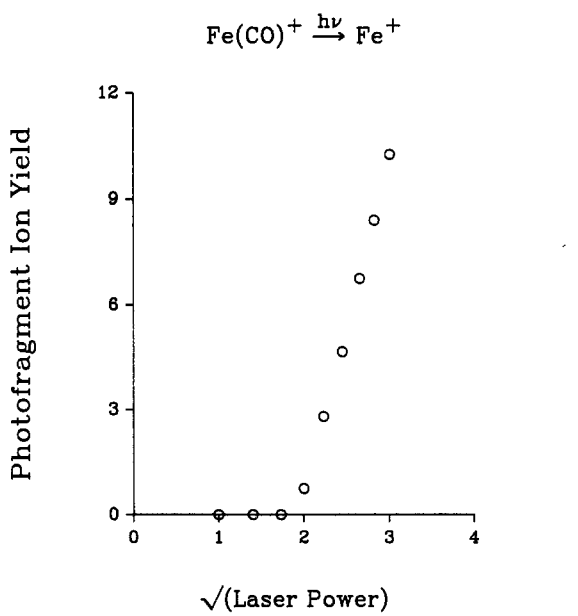

Figure 5. Coaxial photofragment ion yield for the photodissociation of $Fe(CO)^+ \rightarrow Fe^+$ as a function of the square root of the laser power ($W^{0.5}$). (λ = 514.5 nm).

idea in mind. For instance, strong effects on the photodissociation of $Fe(CO)_yL^+$ are observed for different L groups, e.g., L = NO, I, I_2, etc.[31]

Freiser et al. have reported photodissociation data for $Fe(CO)^+ \rightarrow Fe^+ + CO$.[27] The authors found that $Fe(CO)^+$ photodissociates over the entire UV–visible wavelength range (225–700 nm). They observe large photodissociation intensities in the UV and a low intensity photodissociation tail at visible wavelengths (400–700 nm). This is contradictory with the results presented here. We find that the $Fe(CO)^+$ ion does not photodissociate in the wavelength range 458–514.5 nm in a crossed laser–ion beam configuration. One possible explanation for the differences between the ICR and ion beam results could be due to a

(31) Bricker, D. L.; Russell, D. H., unpublished results.

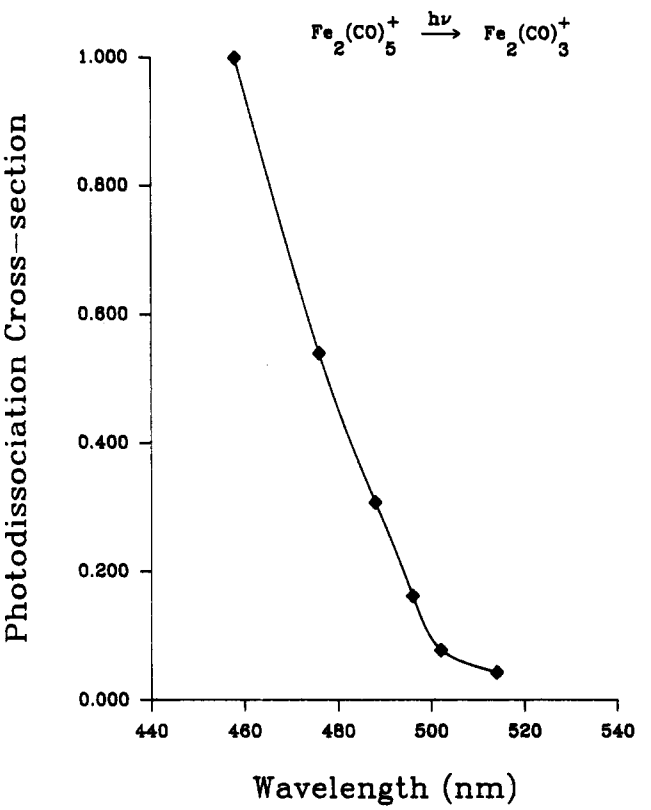

Figure 6. Photodissociation cross section as a function of laser wavelength for $Fe_2(CO)_5^+ \rightarrow Fe(CO)_3^+$.

reduced dynamic range for the crossed laser–ion beam photodissociation technique. This may especially be true since high-resolution mass selection attenuates the number of photofragment ions transmitted through the second electrostatic analyzer. The dynamic range limitation was examined, however, by attempting to photodissociate the $Fe(CO)^+$ ion derived from electron impact of $Fe(CO)_5$ neutral (instead of $Fe_3(CO)_{12}$ neutral) in a cross laser–ion beam configuration in the third field-free region of the mass spectrometer. Although collector signals for pro-

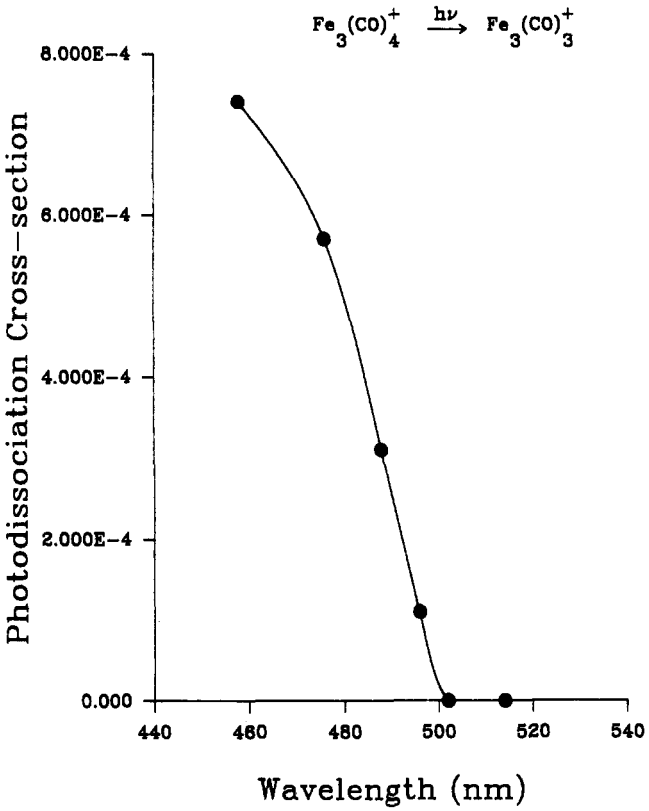

Figure 7. Photodissociation cross section as a function of laser wavelength for $Fe_3(CO)_4^+ \rightarrow Fe_3(CO)_3^+$.

duction of the $Fe(CO)^+$ ion (from the electron impact of $Fe(CO)_5$) were found to be nearly 3 orders of magnitude larger than those in the high-resolution study, photodissociation of the $Fe(CO)^+$ ion was not observed. Thus, the absence of photodissociation signal in the high-resolution study is definitely not due to dynamic range limitations.

The most likely explanation for the differences between the FT-ICR and laser-ion beam photodissociation results for $Fe(CO)^+$ are (i) because the ions are trapped and irradiated for long periods of time (ca. 8 s) in the ICR cell, photodissociation occurs by a sequential two photon process or (ii) the slow rate of decay for a spin-forbidden dissociation process precludes observation by the microsecond beam apparatus, but the longer time scale of the ICR is sufficient for dissociation to occur. Although the data contained in Figure 5 clearly indicate that a two-photon photodissociation of $FeCO^+$ occurs in the coaxial laser-ion beam photodissociation experiment, this does not rule out the occurrence of a slow spin-forbidden photodissociation channel. More detailed experiments on this question are in progress.

Loss of two carbonyls from $Fe_2(CO)_5^+$ to yield $Fe_2(CO)_3^+$ is found to have the largest photodissociation cross section (λ_{max} = 458 nm) (see Figure 6) for all the $Fe_x(CO)_y^+$ ions examined. Photodissociation of $Fe_2(CO)_5^+$ to form $Fe_2(CO)_3^+$ is unusual because the photofragment ion yield decreases by ca. 2 orders of magnitude on going from 458 to 514.5 nm. Although the photodissociation cross section at 514.5 nm is small, the photodissociation signal is still measurable and does not reach threshold.

Photodissociation of the $Fe_3(CO)_4^+$ ion (Figure 7) yields $Fe_3(CO)_3^+$ exclusively. The loss of one carbonyl ligand from the iron metal center is unusual. In our previous study of $Fe_3(CO)_y^+$ ions (y = 5–12), loss of a single ligand was not observed except for y = 9 and 10, and only in the case of the $Fe_3(CO)_9^+$ ion was the loss of one carbonyl a dominant reaction channel.[17] The photodissociation cross section for the $Fe_3(CO)_4^+$ ion is small at all wavelengths; e.g., relative photodissociation cross sections vary from 7.4 $\times 10^{-4}$ at λ = 458 nm to 1.1 $\times 10^{-4}$ at λ = 496 nm, and no photodissociation signal is detectable at 502 and 514.5 nm. We assign a threshold energy for photodissociation of $Fe_3(CO)_4^+$ at 502 nm yielding a bond dissociation energy of 57 kcal/mol. The assigned threshold for $Fe_3(CO)_4^+ \rightarrow Fe_3(CO)_3^+$ implies that the $Fe_3(CO)_4^+$ ion is extremely stable with respect to the $Fe_3(CO)_3^+$ ion; i.e., the metal carbonyl bonds of the $Fe_3(CO)_4^+$ system are unusually strong.

The stability of the $Fe_3(CO)_4^+$ ion relative to other $Fe_3(CO)_y^+$ ions is supported by complimentary information derived from the high-resolution, collision-induced dissociation (CID) data of various $Fe_3(CO)_y^+$ ions. For example, Figure 8 contains the CID spectra for the $Fe_3(CO)_{10}^+$ ion. Note the unusually large CID signal corresponding to the production of the $Fe_3(CO)_4^+$ daughter ion. One feature common to all the CID spectra of iron cluster fragment ions is that loss of one carbonyl ligand is always the dominant reaction channel, and the relative abundances of the iron carbonyl ions, corresponding to successive carbonyl losses, decrease in a monotonic fashion (e.g. -1 CO > -2 CO > -3 CO etc.). The exception to this trend is the $Fe_3(CO)_4^+$ ion. Collision-induced dissociation of the $Fe_3(CO)_y^+$ ions (for y = 5–12) also reveal anomously large $Fe_3(CO)_4^+$ ion intensities suggesting the $Fe_3(CO)_4^+$ ion has an uncommon stability. This stability may be rationalized in terms of a different type of iron metal center-to-ligand bonding. The carbonyl ligands in the $Fe_3(CO)_4^+$ ion may be bridging (two-electron or four-electron donors to the metal center) rather than terminal CO groups which have lower binding energies.

The only other iron carbonyl fragment ions examined that undergo photodissociation via loss of one carbonyl ligand are the $Fe_3(CO)^+$, and $Fe_2(CO)^+$ ions (see Tables I and II). For both of these ions the photodissociation threshold occurs at approximately 514.5 and 488 nm, respectively. The relatively large metal carbonyl binding energies in these ions may also imply that the carbonyl ligands are bonded in a bridging fashion. The electron deficiencies of the bare metal iron cluster ions (Fe_3^+ and Fe_2^+) are large with respect to more fully ligated system. Hence, to reduce this electron deficiency, iron carbonyl ions with few ligands (e.g., $Fe_3(CO)^+$, $Fe_2(CO)^+$, and $Fe(CO)^+$) may form bridging ligand complexes with the metal center, or alternatively the metal center (or atom) may bond with both the carbon and oxygen atoms of the carbonyl ligands. This latter idea is supported by results from this laboratory which indicate that both iron carbide and iron oxide ions are produced by the collision-induced dissociation of singly ligated iron carbonyl ions.[32] Thus, the idea of bridging carbonyl groups or unusual metal carbonyl bonding for certain iron carbonyl ions may explain why their photodissociation and CID spectra appear anomalous. This type of Fe···CO interaction may also explain why $Fe(CO)^+$ does not photodissociate to Fe^+ in the visible wavelengths.

Photodissociation of Fe_3^+ leads to the formation of the Fe_2^+ ion exclusively (see Figure 9). A photodissociation threshold for Fe_3^+ is not observed in the blue-green wavelength regions. Thus, the photodissociation reaction $Fe_3^+ \rightarrow Fe_2^+ + Fe$ has an energy requirement of less than 2.43 eV. If a linear structure for the Fe_3^+ ion is assumed, an upper limit to the iron–iron bond dissociation energy of <56 kcal/mol is obtained (see Table II). However, if the structure of the Fe_3^+ ion is triangular, an upper limit

(32) Tecklenburg, R. E., Jr.; Russell, D. H., unpublished results.

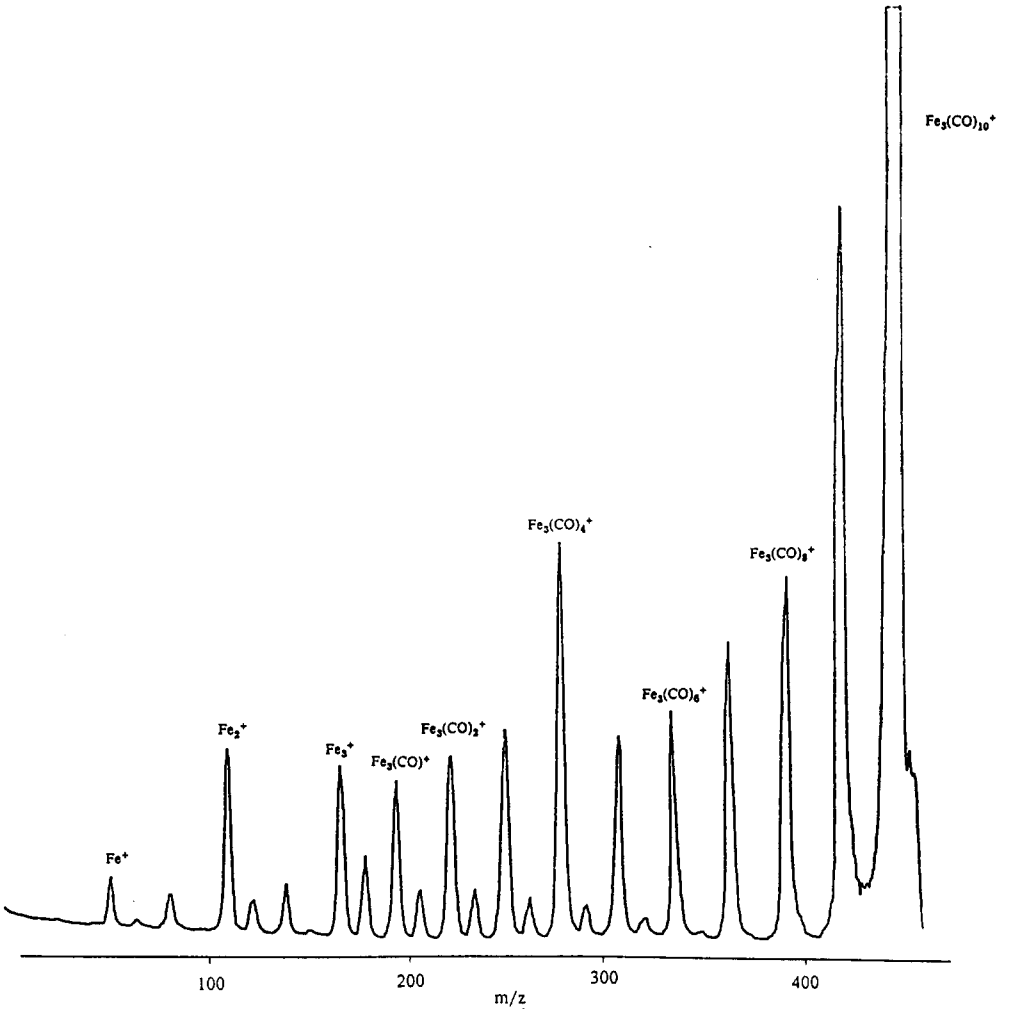

Figure 8. The $Fe_3(CO)_{10}^+$ ion activated by 8-keV high-energy collisions with helium target gas. Note the large signal intensity for production of the $Fe_3(CO)_4^+$ daughter ion.

to the average iron–iron bond dissociation energy is 28 kcal/mol. This latter value for the iron–iron bond strength falls within the lower end of a range of energies Smalley et al. measured for the photodissociation threshold for $Fe_3^+ \rightarrow Fe_2^+ + Fe$ (26.9–50.3 kcal/mol).[18] The Fe_2^+ ion does not photodissociate even at the highest energy used (458 nm); therefore, we assign a lower limit of >62.4 kcal/mol to the iron–iron bond dissociation energy. This lower limit for the Fe^+–Fe bond strength in the Fe_2^+ ion is in good agreement with measurements from complimentary techniques for determination of metal–metal bond strengths. For example, Freiser et al. reported a value for $D(Fe–Fe)^+$ between 58 (±5) and 69 (±5) kcal/mol[33] obtained by CID bracketing techniques and a Fe^+–Fe bond dissociation energy of 62 (±5) kcal/mol by photodissociation.[34] Smalley et al. estimated the bond strength of Fe_2^+ (based on the photodissociation threshold for the Fe_2^+ ion) to be in the range 56.0–67.3 kcal/mol.[18]

It is interesting to compare the bond dissociation energy for the Fe_2^+ ion and Fe_2 neutral. Bond dissociation energies reported for Fe_2 neutral are, in general, much smaller than the iron–iron bond strength in the Fe_2^+ ion determined by ICR and ion beam photodissociation methods. For example, $D^0(Fe–Fe)$ has been reported to be 19 ± 7 kcal/mol by Lin and Kant[35] and 18 ± 4 kcal/mol by Shim and Gingerich.[36] The much larger bond dissociation energy of Fe_2^+ as compared to Fe_2 neutral may arise from the fact that ionization of Fe_2 neutral involves removal of an electron from a strongly antibonding orbital. This explanation, however, is contradictory to negative ion photoelectron studies of Fe_2^- which have demonstrated that the Fe_2^- anion has slightly larger bond lengths and lower vibrational frequencies than Fe_2 neutral.[37] These results suggest that detachment of the electron in Fe_2^- must arise from slightly antibonding molecular orbitals. Hence, ionization of Fe_2 neutral is not expected to occur by removing a strongly antibonding electron. Thus, one would not expect the bond dissociation energy of Fe_2^+ to be substantially larger than that of Fe_2.

The differences in bond strengths between Fe_2 and Fe_2^+ raises important questions concerning the bonding in the two species. Bond energies based upon photodissociation are subject to inherent limitations. That is, in order to accurately measure the bond strength for Fe_2^+, an excited electronic state (S_j) must lie close to the dissociation threshold. If S_j lies above the dissociation threshold, the measured bond dissociation energy will be high. Another potential problem with the photodissociation technique stems from the fact that other energy loss mechanisms can compete with the dissociation process, e.g., radiative decay. If at low photon energies the rate for radiative decay is much greater than the rate for cleavage of the iron–iron

(33) Jacobson, D. B.; Freiser, B. S. *J. Am. Chem. Soc.* **1984**, *106*, 4623.
(34) Hettich, R. L.; Freiser, B. S. *J. Am. Chem. Soc.* **1987**, *109*, 3537.
(35) Lin, S. S.; Kant, A. *J. Phys. Chem.* **1969**, *73*, 2450.
(36) Shim, I.; Gingerich, K. A. *J. Chem. Phys.* **1982**, *77*, 2490.
(37) Leopold, D. G.; Lineberger, W. C. *J. Chem. Phys.* **1986**, *85*, 51.

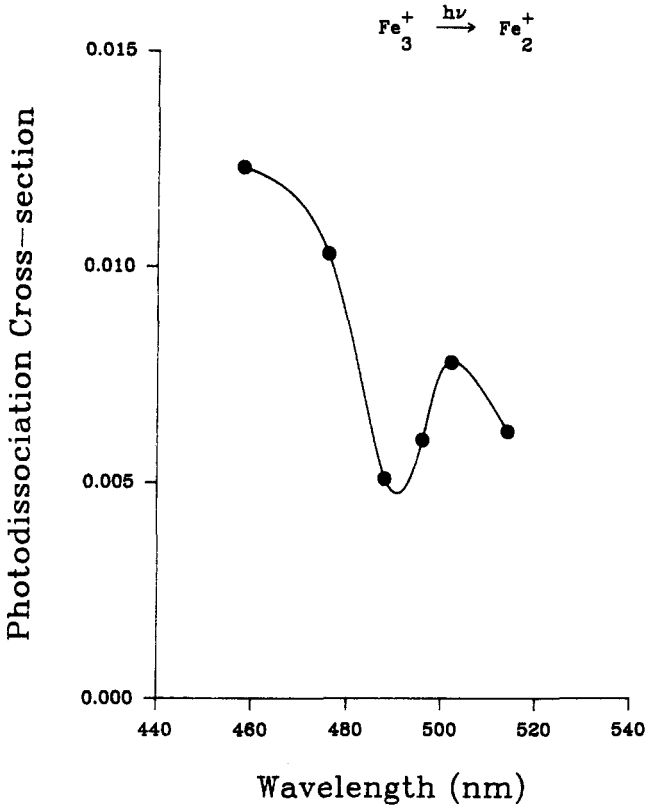

Figure 9. Photodissociation cross section as a function of laser wavelength for $Fe_3^+ \rightarrow Fe_2^+$.

bond, then no Fe^+ photoproduct ions will be observed. As the photon energy is increased, the rate for photodissociation may become comparable to the rate for emission of a photon. This will also lead to anomalously high values for the measured Fe_2^+ bond strength. Competitive radiative decay/photodissociation pathway may explain why the photodissociation cross sections steadily decrease on going from the $Fe_2(CO)_5^+$ ion to the Fe_2^+ ion (see Table I), i.e., slow radiative decay processes at low M/L ratios and fast radiative decay processes at high M/L ratios. Additional studies are underway which hopefully will resolve some of these questions.

Conclusions

The high-resolution and large dynamic range capabilities of the laser–ion beam mass apparatus allow the electronic and thermodynamic properties of novel ionic transition-metal cluster fragments to be studied without complicating solvation effects. Although much higher mass resolutions (R = 100 000–150 000) are obtainable by using a double-focusing mass spectrometer of the sort described herein, these resolutions result in poor ion transmission efficiencies. As a result, laser–ion beam photodissociation methods may be limited to moderate resolutions (5000–50 000) since data acquisition times become prohibitively long at higher mass resolutions.

Acknowledgment. We wish to express our appreciation to one of the reviewers for bringing ref 29 to our attention. This work was supported by grants from the U.S. Department of Energy, Office of Basic Energy Sciences (DE-AS05-82ER13023), and the National Science Foundation (CHE-8418457).

Registry No. $Fe_3(CO)_{12}$, 17685-52-8; Fe_3^+, 73145-64-9; Fe_2^+, 61674-68-8; $Fe(CO)_4^+$, 35038-17-6; $Fe(CO)_3^+$, 35038-16-5; $Fe(CO)_2^+$, 35038-15-4; $Fe(CO)^+$, 35038-14-3.

Mono(cyclooctatetraenyl) Actinide Complexes. 1. Preparation of the Diamides $(C_8H_8)An[N(SiMe_3)_2]_2$ (An = Th, U) and the Structure of $(C_8H_8)Th[N(SiMe_3)_2]_2$

Thomas M. Gilbert, Robert R. Ryan, and Alfred P. Sattelberger*

Inorganic and Structural Chemistry Group (INC-4), Isotope and Nuclear Chemistry Division, Los Alamos National Laboratory, Los Alamos, New Mexico 87545

Received April 7, 1988

An improved synthesis of the mono(cyclooctatetraenyl)thorium ("half-sandwich") complex $(C_8H_8)ThCl_2(THF)_2$ (**1a**) is reported. Although treatment of **1a** or the uranium analogue $(C_8H_8)UCl_2(THF)_2$ (**1b**) with alkyllithium or Grignard reagents leads to intractable products, metathesis of the chloride ligands of **1a** or **1b** with 2 equiv of $NaN(SiMe_3)_2$ cleanly gives the pseudo-seven-coordinate diamide complexes $(C_8H_8)An[N(SiMe_3)_2]_2$ (An = Th, **2a**; An = U, **2b**). A single-crystal X-ray diffraction study of $(C_8H_8)Th[N(SiMe_3)_2]_2$ (T = 298 K, monoclinic, $P2_1/a$, a = 12.071 (2) Å, b = 13.160 Å, c = 18.113 Å, β = 90.96°, V = 2876.9 Å^3, Z = 4) revealed that one carbon of each silyl amide ligand is directed toward the thorium in such a way as to mimic a four-legged piano stool with trans nitrogen atoms and trans carbon atoms. This result is ascribed to the coordination number deficiency at the metal center. The amide complex **2a** does not react with H_2 even at elevated temperatures.

Introduction

In 1980, the first mono(cyclooctatetraenyl)thorium ("half-sandwich") complexes were reported. The parent compound $(C_8H_8)ThCl_2(THF)_2$ (**1a**) was prepared by prolonged (ca. 1 week) reaction of thorocene with thorium tetrachloride in refluxing THF (eq 1) and its structure

$$(C_8H_8)_2Th + ThCl_4 \xrightarrow[\Delta]{THF} \underset{\mathbf{1a}}{2(C_8H_8)ThCl_2(THF)_2} \quad (1)$$

determined by single-crystal X-ray diffraction.[1,2] In the

0276-7333/88/2307-2514$01.50/0